THE ASTRONOMICAL JOURNAL VOLUME 75, NUMBER 6 AUGUST 1970

Self-Consistent Models of Elliptical Galaxies

KEVIN H. PRENDERGAST
Department of Astronomy, Columbia University, New York

AND

EUGENE TOMER
Ole Rømer Observatory, Aarhus, Denmark

(Received 11 February 1970)

Rotating, stationary models of elliptical galaxies are constructed using a Maxwellian distribution function modified by an energy cutoff. The Liouville equation and a nonlinear Poisson equation are solved simultaneously by an uncommon technique. The computed models are bounded and have many of the standard observed features. Comparison is made with NGC 3379.

I. INTRODUCTION

BECAUSE of their smooth appearance and evident simplicity, elliptical galaxies would seem to be natural choices for the application of classical stellar dynamics. This very simplicity, however, limits the kind of observational material that one can extract. One therefore needs rather accurate photometric data in order to distinguish between the various possible theories. Many ellipticals show a very high degree of central condensation while the outer envelopes, the regions where theories are likely to differ, may have intensities considerably below the level of the night sky, which, for instance, is the case in NGC 3379 (Miller and Prendergast 1962). There are theoretical difficulties as well. Since we know very little about the evolution of large stellar systems, we have to stop short of finding a distribution function $f(t,\mathbf{r},\mathbf{v},m)$ and the collective gravitational potential $\psi(t,\mathbf{r})$. One usually offers relaxation arguments, declares encounters unimportant for short times, and perhaps one makes a few other idealizations, then constructs a stationary model. All such models so far are spherical with one exception (Lynden-Bell 1962), for in spite of all these simplifying assumptions, there are still difficulties in making stationary, rotating models.

We shall also assume that f and ψ are time independent, that is, the model so constructed is *stationary*, and we assume moreover that all stars have the same mass. We note that very little can be learned about f from observations, unfortunately, at least in the case of NGC 3379 (Miller 1963). The customary approach has been to take a good guess at $f(E_1,E_2,\cdots)$ where E_1, E_2, $\cdots$ are integrals of motion for a single star; this is also our approach.

II. FORMULATION

Concerning the distribution function, let us take

$$f(E,J)=\alpha\exp\left(-\frac{1}{m\sigma^2}E+\beta J\right), \qquad (1)$$

where E and J are the energy and angular momentum integrals for a single star of mass m, α and β are constants, and σ is a dispersion parameter. In choosing a one-particle distribution function we are motivated by the relatively small color change $\Delta(B-V)\sim 0.06$ observed in NGC 3379 from the center outward. In the case of NGC 3115 the rather large color change indicated that a one-population model is probably insufficient (Miller and Prendergast 1968).

As it now stands, f is Maxwellian in velocity space. Let $\mathbf{r}$ and $\mathbf{v}$ denote the position and velocity vectors. Then if $\psi(\mathbf{r})$ is the potential per unit mass, the integrals of motion take the form

$$E=\tfrac{1}{2}mv^2+m\psi(\mathbf{r}), \quad J=(\mathbf{r}\times m\mathbf{v})_z,$$

where the subscript refers to the z component. Since f is given as a function of the integrals of motion, it satisfies Liouville's equation *a fortiori* (usually called Jeans theorem), and the problem now is to find a solution to the nonlinear Poisson equation $\nabla^2\psi=4\pi\gamma d(\mathbf{r},\psi)$. The equation is nonlinear because the density d is given by

$$d(\mathbf{r},\psi)=m\int_{E\leqslant -C} f(E,J)d\mathbf{v}, \qquad (2)$$

where $d\mathbf{v}$ is the 3-dimensional volume element in velocity space and $C>0$ is a constant, the cutoff energy. We impose the usual boundary condition that $\psi\rightarrow 0$ as $r\rightarrow\infty$. Models so constructed are called *self consistent*; thus, each star moves in the smoothed, collective gravitational field of all the other stars. This is not the only way to construct self-consistent models but it is evidently the simplest. Also, we do not consider a possible third integral of motion when specifying f. The existence of a third isolating integral will restrict the orbits to a still smaller subset of the energy surface.

The cutoff of the distribution function f for energies greater than $-C$ is of the "sharp" type, in contrast to the "gradual" type obtained, not by truncating f at $E=-C$, but by allowing f to go smoothly to zero. This has important consequences at the outer envelope. At any fixed $\mathbf{r}$ the inequality $E\leqslant -C$ defines a spherical region in velocity space given by

$$0 \leqslant v^2 \leqslant \left\{ -\frac{2C}{m} - 2\psi(\mathbf{r}) \right\},$$

over which the integral in (2) is taken. We observe that when

$$\psi(\mathbf{r}) + \frac{C}{m} = 0, \tag{3}$$

we have $v^2=0$ and hence no orbit can extend beyond the surface defined implicitly by (3). It is convenient to call this surface the boundary of the galaxy and we note that the boundary is not known at the outset. At any rate there is no evaporation problem because every star has energy $E \leqslant -C < 0$ and therefore none can escape the system. It is evident that some kind of cutoff is necessary for a Maxwellian distribution because arbitrarily large velocities are not physically meaningful, nor are the infinite radii and infinite masses obtained by some of the earlier theories. If one still insists on an f of the form in Eq. (1), then a more refined type of cutoff for a particular galaxy could, for instance, take into account the potential fields of the various neighbors of the galaxy concerned, but then in this case one is no longer justified in considering an equilibrium situation, in general. For the sake of constructing a definite rotating, equilibrium model, we have therefore introduced the sharp cutoff.

Thus, we are led to seek a solution ψ of the nonlinear, elliptic partial differential equation,

$$\nabla^2\psi = 4\pi\gamma m \int_{E \leqslant -C} \alpha \exp\left(-\frac{1}{m\sigma^2} E + \beta J \right) d\mathbf{v},$$

with the boundary condition $\psi \to 0$ as $r \to \infty$. In addition, we also prescribe the condition $\psi \to -A/m$ as $r \to 0$, where $A>0$ is a given constant; that one can do this is not obvious. In any case, one must solve the Poisson equation in the interior of the "free" boundary surface, the Laplace equation in the exterior; at the free surface itself, ψ and its normal derivative must be continuous. It is not possible to consider the interior and exterior problems separately. Before proceeding further, we eliminate the various unessential constants by the common device of a dimensional analysis.

III. DIMENSIONAL ANALYSIS

Asterisk subscript denotes cgs-dimensioned quantity (constant, variable, operator); no subscript denotes dimensionless quantity. We consider for given $A_* > 0$ the following problem for ψ_*:

$$\nabla_*^2\psi_* = 4\pi\gamma_* m_* \int_{E_* \leqslant -C_*} \alpha_* \exp\left(-\frac{1}{m_*\sigma_*^2} E_* + \beta_* J_* \right) d\mathbf{v}_*,$$

$$\psi_* \to -A_*/m_* \text{ as } r_* \to 0, \quad \psi_* \to 0 \text{ as } r_* \to \infty.$$

A scalar magnification $(\mathbf{r}_*, m_*, t_*) \to (\mathbf{s}, m, t)$ of the independent variables will now be made according to

$$\left.\begin{aligned} \mathbf{r}_* &= L_*\mathbf{s} \\ m_* &= M_* m \\ t_* &= T_* t \end{aligned}\right\}, \tag{4}$$

where L_*, M_*, T_* are certain cgs-dimensioned units of length, mass, time to be chosen presently, while $\mathbf{s}$, m, t are real quantities, usually called the *dimensionless variables*. It is easy to see that all other constants, variables and operators must transform according to (4). For instance, $\alpha_* = L_*^{-6}T_*^3\alpha$, $\psi_* = L_*^2 T_*^{-2}\psi$, and $\nabla_*^2 = L_*^{-2}\nabla^2$. Consider in particular

$$\gamma_* = L_*^3 M_*^{-1} T_*^{-2}\gamma,$$
$$\sigma_* = L_* T_*^{-1}\sigma,$$
$$m_* = M_* m.$$

We can eliminate three constants at once by putting $m=\sigma=\gamma=1$. It follows that the scale factors are $L_* = m_*\gamma_*\sigma_*^{-2}$, $M_* = m_*$, $T_* = m_*\gamma_*\sigma_*^{-3}$ and the dimensionless problem becomes

$$\nabla^2\psi = 4\pi\alpha \int_{E \leqslant -C} \exp(-E + \beta J) d\mathbf{v}, \tag{5}$$

$$\psi \to -A \text{ as } s \to 0, \quad \psi \to 0 \text{ as } s \to \infty, \tag{6}$$

where $E = \frac{1}{2}v^2 + \psi$ and $J = (\mathbf{s} \times \mathbf{v})_z$. Of course

$$A_* = L_*^2 M_* T_*^{-2} A,$$

etc. The free surface is now described by $\psi(\mathbf{s}) + C = 0$.

Presumably, because of the cutoff in the distribution function, the configuration has a finite dimensionless radius R. For convenience in the numerical work we rescale the radial coordinate so that the model lies within the unit sphere in the new variable.

Introduce the potential

$$U(\mathbf{r}) = \psi(R\mathbf{r}) + C.$$

We observe that the free surface is now described by $U(\mathbf{r})=0$ and that $0 \leqslant r \leqslant 1$ implies that $0 \leqslant Rr \leqslant R$. The dimensionless problem for U, which we will treat numerically, is the following:

$$\nabla^2 U = 4\pi\alpha R^2 \exp C \int_{\frac{1}{2}v^2 + U \leqslant 0} \exp(-\tfrac{1}{2}v^2 - U + \eta I) d\mathbf{v}, \tag{7}$$

$$U \to C \text{ as } r \to \infty, \quad U \to C - A \text{ as } r \to 0, \tag{8}$$

where $I = (\mathbf{r} \times \mathbf{v})_z$, $\eta = \beta R$ while α and v have the same meaning as before. We note that $C-A$ must be negative and this implies that $A > C > 0$.

At this point we encounter two subtleties of this problem. Suppose we assign values to C and to η, and the combination αR^2 and attempt to solve (7). The solution of this problem does not appear to exist. Rather it seems that (7) is an eigenvalue problem with

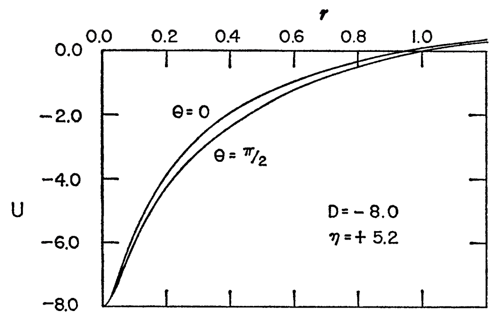

FIG. 1. Potential $U(r,\theta)$.

αR^2 as an eigenvalue to be determined if C and η alone are given. The second subtlety occurs when we consider a sequence of models with $\eta=0$, C increasing. It is found that no solution exists for C larger than a certain maximum value, corresponding to a particular value of U at the origin, and to a particular degree of central condensation. We know, however, that the spherically symmetric problem with $\eta=0$ has solutions for any degree of central concentration, which can easily be found by integrating an ordinary differential equation from the center outwards for assigned U at the origin. We have done this and found that C is *not* a monotonic function of the central potential. It appears, then, that we must prescribe U at the origin, treat $4\pi\alpha R^2 \exp C$ as an eigenvalue and determine C *a posteriori* when and if a solution is obtained.

IV. EIGENVALUE PROBLEM

Let r, θ, φ denote spherical coordinates and v_r, v_θ, v_φ denote the corresponding velocity components. We may then write $I=(\bar{r}\times\bar{v})_z=rv_\varphi \sin\theta$. If we put

$$\rho(r,\theta;\, U)=\int_{\frac{1}{2}r^2+U\leqslant 0} \exp(-\tfrac{1}{2}v^2-U+\eta r v_\varphi \sin\theta)\,dv_r dv_\theta dv_\varphi,$$

$$\lambda=4\pi\alpha R^2 \exp C,$$

then we have to deal with the eigenvalue problem for λ and $U(r,\theta)$,

$$\nabla^2 U=\lambda\rho(r,\theta;\, U). \qquad (9)$$

By forcing the free surface to reside within the unit sphere, we may no longer prescribe *both* conditions in (8), for these conditions now become dependent as will be shown in the Appendix. We prescribe instead

$$U(0,\theta)=D, \quad U(1,\pi/2)=0, \qquad (10)$$

where $D<0$, and the second condition is simply the statement that the free surface has an equational radius of one. An iterative solution of this free-boundary, eigenvalue problem is given in the Appendix. Our numerical results indicate that Eq. (9) together with boundary conditions (10) is a well-posed problem. Naturally, η must also be given.

V. RESULTS

Two parameters are needed to specify the dimensionless model uniquely, the central potential D, and the rotation parameter η. For a range of values of these two parameters, solutions $U(r,\theta)$ of Eq. (9) satisfying boundary conditions (10) were found numerically on a grid of eight angular points $0\leqslant\theta_j\leqslant\pi/2$ and about 50 radial points $0\leqslant r_k\leqslant 1$. Of course the eigenvalue λ was also computed. From the solution $U(r,\theta)$ the dimensionless density $\lambda\rho(r,\theta;\, U(r,\theta))$ was computed on the same grid of points as well as other quantities such as the projected density and rotation curves.

Figures 1 and 2 show the potential U and density $\lambda\rho$ for typical cases. A homologous sequence of models was found in the range $-1\leqslant D<0$, as one could expect from the power-series expansion of the density (by a standard device, the expression for ρ can be written as a single integral). Central condensation becomes greater as the potential well becomes deeper; and as the rotation parameter is increased from zero, the models become progressively flatter; $\eta=0$ gives spherical models.

Figure 3 shows typical isophotal contours obtained by projecting the density $\lambda\rho$ along the x axis and assuming constant mass-to-light ratio. The contours look more or less elliptical in shape. It is difficult to produce more pancake-looking contours because this sequence naturally terminates at the point where the angular momentum is so large that the models fly apart. In general, this point was reached at an axial ratio of about 3 to 1. Also, our numerical scheme was best suited for round objects. At certain values of D it was even possible to produce a density minimum at the center by spinning the galaxy fast enough (large η), but we were unable to manufacture doughnuts.

For various rotation parameters η, Fig. 4 gives the ellipticity. These curves are in general agreement with observed ellipticity variation for ellipticals (Liller

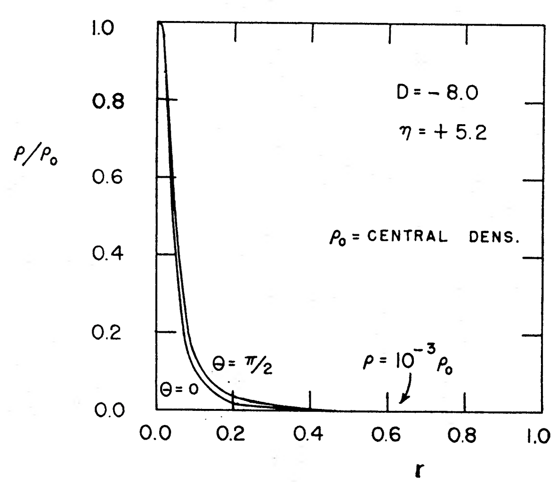

FIG. 2. Relative density: When $\eta=+3.0$, the two curves lie much closer together; they coincide when $\eta=0$.

1960). A common feature is that isophotes become more spherical in the outer envelope, a feature that is not surprising. The curves are not supposed to suggest that ϵ should go to zero at the center of the model.

Some rotation curves are given in Fig. 5. The rotational velocity $\langle v_\phi \rangle$ vanishes at the edge of the galaxy because of the cutoff, and the need for the cutoff has already been emphasized. In a rotating coordinate system these results will be different but we did not investigate this.

In Fig. 6 we give computed brightness curves for three values of the central potential D, all for $\eta=3$. The axial ratio of NGC 3379 is about $\frac{7}{8}$ which corresponds roughly to $\eta=3$. The idea is to match the computed and observed brightness curves, thus obtaining a value for D to match NGC 3379. That this can be done at all is rather a bit of luck, due mostly to the linear portion of both brightness curves (King 1966). $D=-8.0$ is the best fit, although a much better one should be obtained at about $D=-10.0$. Unfortunately, we did not compute the case $D=-10.0$; it required a much finer grid of points at the center because of the sharpened density peak. At any rate a spherical model will practically suffice for NGC 3379. We only point out the method used in making a match; in this case there probably is not much room for a serious mismatch.

For the case $D=-8.0$, $\eta=+3.0$, which corresponded most nearly to NGC 3379, Fig. 7 gives the dispersion ratio $(\langle v_\phi^2\rangle - \langle v_\phi\rangle^2)/\langle v_r^2\rangle$. It does not change much throughout the computed model. Therefore the measured dispersion in NGC 3379, which is 187 km/sec at the center and in the line of sight (Burbidge, Burbidge, and Fish 1961), might be typical for the galaxy as a whole.

Because the model is stationary one expects the virial theorem to hold, and we found this to be the case numerically. A dimensionless virial theorem

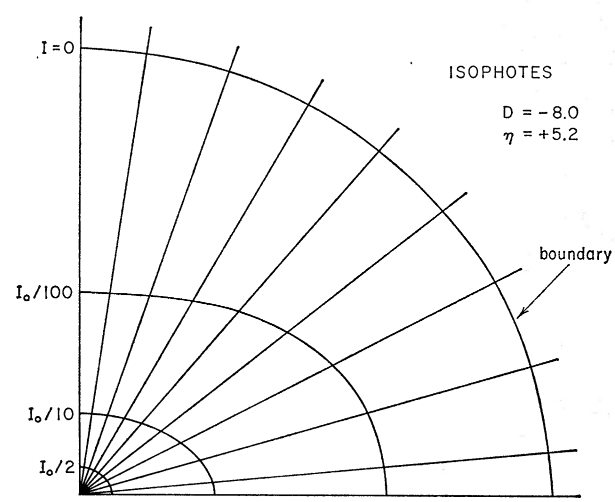

FIG. 3. Isophotes for a moderately flattened model: When $\eta=+3.0$, the isophotes are nearly spherical (see Fig. 4).

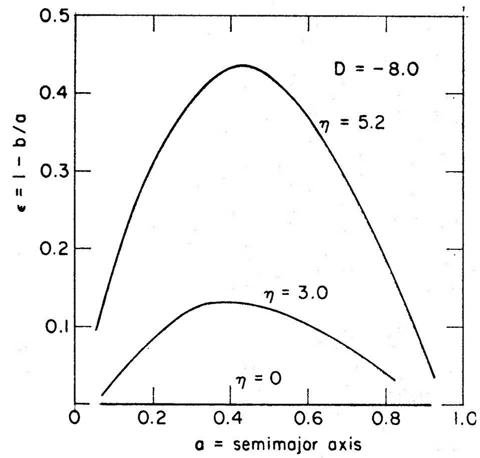

FIG. 4. Ellipticity ϵ for three values of the rotation parameter η.

4KE+2PE$-C$ Mass$=0$ was found to hold to within three or four significant figures, thus providing another numerical check besides the obvious ones. Of course KE includes the kinetic energy of rotation.

Finally, we consider the total mass in cgs units:

$$M_*{}^T = m_* \alpha_* \int_{E_* \leqslant -C_*} \exp\left(-\frac{1}{m_* \sigma_*{}^2} E_* + \beta_* J_*\right) d\mathbf{v}_* d\tau_*,$$

where $d\tau_*$ is the element of volume. Writing

$$m_* = L_* \gamma_*{}^{-1} \sigma_*{}^2, \quad \alpha_* = L_*{}^{-6} T_*{}^3 \alpha,$$

etc., one can easily derive

$$M_*{}^T = \sigma_*{}^2 \gamma_*{}^{-1} \frac{RL_*}{2} \lambda \int \rho d\tau,$$

where $\lambda \int \rho d\tau$ is the mass computed in the dimensionless variables. The expression on the right does not contain m_*. If one knows the distance to the galaxy, then the scale factor RL_* can be read off the observed brightness curve by comparison with the computed brightness curve. Assigning a value to σ_* then determines $M_*{}^T$.

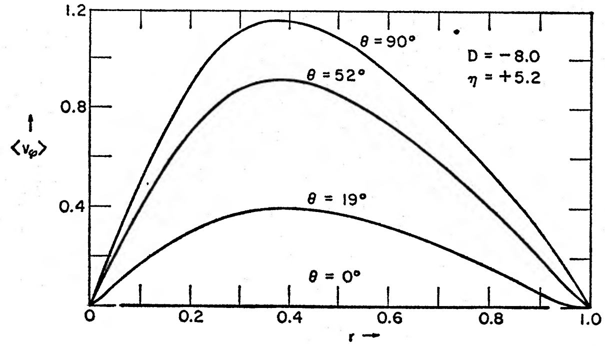

FIG. 5. Rotation curves for moderate flattening.

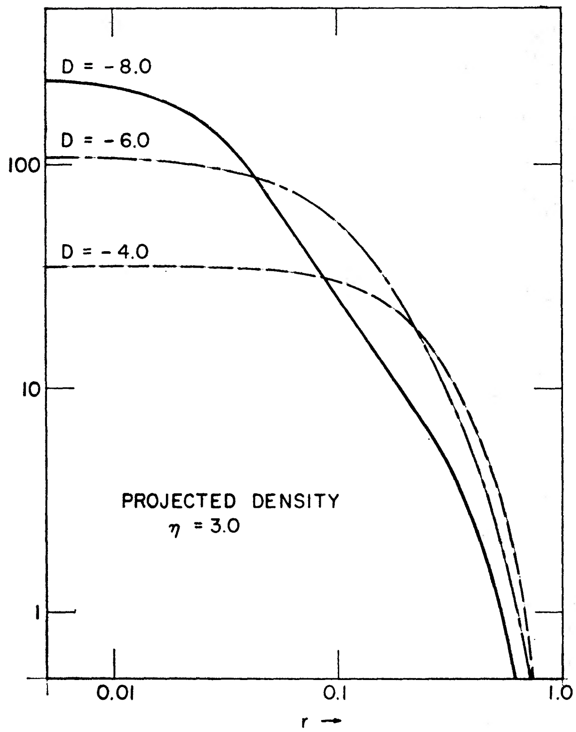

FIG. 6. Computed brightness: In the case $D=-8.0$, the slope of the linear portion of the curve is about $-\frac{3}{2}$, the same as for NGC 3379.

Of course this method of determining the total mass has its own weak assumptions, one of them being the identification of the measured dispersion with the number σ_*. We also assume that the distribution function is approximated by (1).

ACKNOWLEDGMENTS

This research was supported by grants from the National Science Foundation which we gratefully acknowledge. We also wish to thank Dr. Robert Jastrow, director of the Institute for Space Studies, NASA, for his kind hospitality, and for his willingness in providing the excellent computing facilities.

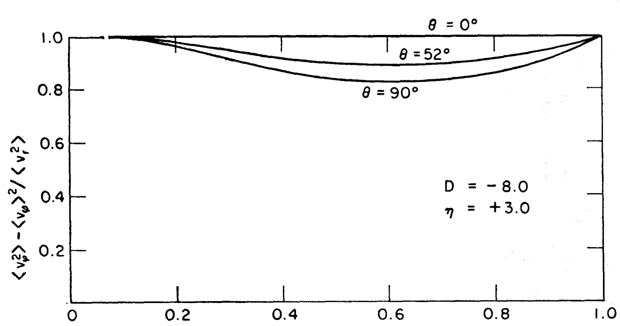

FIG. 7. Dispersion ratio: Note that $\langle v_r\rangle=0$ and that $\langle v_r^2\rangle=\langle v_\theta^2\rangle$ because of symmetry in Eq. (1). When $\eta=0$ the dispersion ratio is 1 everywhere.

APPENDIX

Equation (9) can be solved numerically by iteration. Determine $U^{(n+1)}(r,\theta)$ from $U^{(n)}(r,\theta)$ according to

$$\nabla^2 U^{(n+1)}=\lambda^{(n)}\rho(r,\theta;\, U^{(n)}(r,\theta)), \tag{A1}$$

where $\lambda^{(n)}$ must also be determined at each iteration step and where each iterate $U^{(n)}(r,\theta)$ satisfies the boundary conditions,

$$\left.\begin{aligned} U^{(n)}(0,\theta)&=D\\ U^{(n)}(1,\pi/2)&=0\end{aligned}\right\}. \tag{A2}$$

To solve (A1) numerically one can proceed as follows: expand $U^{(n+1)}(r,\theta)$ and $\rho^{(n)}(r,\theta)\equiv\rho[r,\theta;\, U^{(n)}(r,\theta)]$ in Legendre polynomials,

$$\rho^{(n)}(r,\theta)=\sum_{k=0}^{\infty}\rho_k{}^{(n)}(r)P_k(\mu),$$

$$U^{(n+1)}(r,\theta)=\sum_{k=0}^{\infty}u_k{}^{(n)}(r)P_k(\mu),$$

where $\mu=\cos\theta$ and the sums are over even indices k. Substituting the expansions for $\rho^{(n)}$ and $U^{(n+1)}$ into (A1) one sees that the Laplacian separates, and an application of Legendre's equation leads to

$$\frac{1}{r^2}\frac{d}{dr}\left[r^2\frac{du_k{}^{(n+1)}}{dr}\right]-k(k+1)\frac{u_k{}^{(n+1)}}{r^2}=\lambda^{(n)}\rho_k{}^{(n)},$$

a linear equation for $u_k{}^{(n+1)}(r)$ in terms of $\rho_k{}^{(n)}(r)$. The linearly independent solutions of the homogeneous equation are r^k and r^{-k-1} so that by the variation-of-constants formula,

$$u_k{}^{(n+1)}(r)=\frac{\lambda^{(n)}}{2k+1}\left\{r^k\int_{r_0}^{r}s^{1-k}\rho_k{}^{(n)}(s)ds\right.$$
$$\left.-\frac{1}{r^{k+1}}\int_{r_0'}^{r}s^{k+2}\rho_k{}^{(n)}(s)ds+A_kr^k+\frac{B_k}{r^{k+1}}\right\},$$

where r_0, r_0', A_k, B_k are constants to be determined as follows: since $U^{(n+1)}$ must be well defined as $r\to\infty$, then $u_k{}^{(n+1)}(\infty)=0$ for $k=2, 4, \cdots$ so we must have

$$A_k=-\int_{r_0}^{\infty}s^{1-k}\rho_k{}^{(n)}(s)ds,$$

and similarly since $U^{(n+1)}$ must be well defined as $r\to 0$, then $u_k{}^{(n+1)}(0)=0$ for $k=2, 4, \cdots$ so we must have

$$B_k=-\int_{0}^{r_0'}s^{k+2}\rho_k{}^{(n)}(s)ds.$$

The latter relation must also hold for $k=0$ for otherwise $u_0{}^{(n+1)}(r)$ would have a singularity at $r=0$. A_0 is determined from the condition $u_0^{(n+1)}(0)=D$,

$$A_0=\frac{D}{\lambda^{(n)}}-\int_{r_0}^{0} s\rho_0^{(n)}(s)ds.$$

Summing $u_k^{(n+1)}(r)P_k(\mu)$ over even indices k, one finds for the solution to (A1)

$$\begin{aligned}U^{(n+1)}(r,\theta)&\\ =D+\lambda^{(n)}\left[\int_0^r s\rho_0^{(n)}(s)ds-\frac{1}{r}\int_0^r s^2\rho_0^{(n)}(s)ds\right]&\\ -\lambda^{(n)}\sum_{k=2}^{\infty}\frac{P_k(\mu)}{2k+1}\left[r^k\int_r^{\infty} s^{1-k}\rho_k^{(n)}(s)ds\right.&\\ \left.+\frac{1}{r^{k+1}}\int_0^r s^{k+2}\rho_k^{(n)}(s)ds\right].&\quad\text{(A3)}\end{aligned}$$

If we consider the second of the conditions (A2), then from (A3) we find

$$\lambda^{(n)}=D\left[-\int_0^1 s\rho_0^{(n)}(s)ds+\sum_{k=0}^{\infty}\frac{P_k(0)}{2k+1}\int_0^1 s^{k+2}\rho_k^{(n)}(s)ds\right]^{-1}.$$

Let us write

$$C^{(n)}\equiv\lim_{r\to\infty} U^{(n+1)}(r,\theta).$$

Taking the limit in (A3) it follows that

$$C^{(n)}=D+\lambda^{(n)}\int_0^1 s\rho_0^{(n)}(s)ds.$$

This shows how conditions (8) become dependent when one introduces the eigenvalue λ, for we expect $C^{(n)}\to C$ as $n\to\infty$.

A Gauss–Legendre quadrature was used to evaluate the integrals in (A3) so this automatically picks out the rays θ_j for the grid. Except for evaluation of the density $\rho^{(n)}$, all numerical operations are reducible to matrix multiplication, so the process is rather efficient. Typical running times on the IBM 360/75 were two seconds per iteration. About 40 iterations were required for convergence to four figures.

REFERENCES

Burbidge, E. M., Burbidge, G. R., and Fish, R. A. 1961, *Astrophys. J.* **134**, 251.
King, I. 1966, *Astron. J.* **71**, 64.
Liller, M. 1960, *Astrophys. J.* **132**, 306.
Lynden-Bell, D. 1962, *Monthly Notices Roy. Astron. Soc.* **123**, 447.
Miller, R. H. 1963, *Astrophys. J.* **138**, 849.
Miller, R. H., and Prendergast, K. H. 1962, *ibid.* **136**, 713.
——. 1968, *ibid.* **153**, 35.